


**AUTHOR QUERY FORM**

	<b>Journal:</b> EA	<b>Please e-mail or fax your responses and any corrections to:</b>
ELSEVIER	<b>Article Number:</b> 16785	<b>E-mail:</b> <a href="mailto:corrections.esil@elsevier.thomsondigital.com">corrections.esil@elsevier.thomsondigital.com</a>
		<b>Fax:</b> +353 6170 9272

Dear Author,

Please check your proof carefully and mark all corrections at the appropriate place in the proof (e.g., by using on-screen annotation in the PDF file) or compile them in a separate list. To ensure fast publication of your paper please return your corrections within 48 hours.

For correction or revision of any artwork, please consult <http://www.elsevier.com/artworkinstructions>.

No queries have arisen during the processing of your article.

Thank you for your assistance.



Contents lists available at ScienceDirect

Electrochimica Acta

journal homepage: [www.elsevier.com/locate/electacta](http://www.elsevier.com/locate/electacta)

## Research highlights

**Effect of  $\text{Al}_2\text{Cu}$  precipitates size and mass transport on the polarisation behaviour of age-hardened Al–Si–Cu–Mg alloys in 0.05 M NaCl***Electrochimica Acta xx (2011) xxx–xxx*

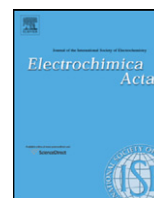
A.C. Vieira\*, A.M. Pinto, L.A. Rocha, S. Mischler

► Influence of the size distribution of Al–Cu phases on the electrochemical behaviour of well defined alloys under controlled mass transport conditions (RDE). ► Oxygen reduction occurs only the  $\text{Al}_2\text{Cu}$  phases. ► Thinner Al–Cu grains the oxygen reduction current deviates at high rotation rates from the Levich behaviour.



Contents lists available at ScienceDirect

Electrochimica Acta

journal homepage: [www.elsevier.com/locate/electacta](http://www.elsevier.com/locate/electacta)

# Effect of Al<sub>2</sub>Cu precipitates size and mass transport on the polarisation behaviour of age-hardened Al–Si–Cu–Mg alloys in 0.05 M NaCl

A.C. Vieira<sup>a,\*</sup>, A.M. Pinto<sup>a</sup>, L.A. Rocha<sup>a</sup>, S. Mischler<sup>b</sup><sup>a</sup> University of Minho, Centre for Mechanics and Materials Technologies (CT2M), 4800-058 Guimarães, Portugal<sup>b</sup> Ecole Polytechnique Fédérale de Lausanne (EPFL), Tribology and Interface Chemistry Group, 1015 Lausanne, Switzerland

## ARTICLE INFO

### Article history:

Received 11 August 2010

Received in revised form 10 February 2011

Accepted 10 February 2011

Available online xxx

### Keywords:

Oxygen reduction

Al<sub>2</sub>Cu precipitates

Mass transport

Age-hardened Al–Si–Cu–Mg

## ABSTRACT

The electrochemical behaviour of age-hardened Al–Si–Cu–Mg alloys was investigated in a 0.05 M NaCl solution under controlled mass transport conditions using a rotating disk electrode. This work aimed at getting better understanding of the effect of the alloy microstructure, in particular the size distribution of Al<sub>2</sub>Cu phase, on the corrosion behaviour of the alloy. Three different size distributions of the Al<sub>2</sub>Cu phase were obtained through appropriate heat treatments. The cathodic reduction of oxygen was found to occur mainly on the Al<sub>2</sub>Cu phases acting as preferential cathodes. Small sized Al<sub>2</sub>Cu phases were found to promote at high rotation rates a transition from a 4 electron to a 2 electron dominated oxygen reduction mechanisms.

© 2011 Published by Elsevier Ltd.

## 1. Introduction

Al–Si hypoeutectic and eutectic casting alloys (containing 6–12% Si) are widely used in the automotive industry, essentially due to their excellent foundry characteristics (castability) and high mechanical properties [1–7]. Nowadays, these alloys became also common in aerospace, transportation and defence industries [3–7]. Copper is commonly added as alloying element to these alloys to improve mechanical strength by precipitation hardening. This process consists in the controlled precipitation of Cu-rich precipitates (usually metastable intermetallic Al<sub>2</sub>Cu phases –  $\theta'$  and  $\theta''$ ) in the Al solid solution during heat treatment. These precipitates constitute obstacles for dislocation movements [5,7,8].

However, the presence of Cu in Al alloys, either as intermetallic phases or in the Al solid solution, has several consequences on the corrosion resistance. First the noble behaviour of Al<sub>2</sub>Cu phase creates a galvanic coupling with the surrounding Al matrix. The Al<sub>2</sub>Cu phase is well known to act as preferential cathode for the oxygen reduction reaction thus, accelerating the oxidation of aluminium [9–11]. Further, the OH<sup>–</sup> produced during oxygen reduction can locally increase the pH, causing the local dissolution of the Al-matrix in the vicinity of the preferential cathodes [10,11]. In such processes, the distribution and the relative surface area of the cathode is expected to influence the corrosion process. However, little is known about the influence on corrosion of the size and distribution

of Cu-containing phases in Al alloys. Liao and Wei [12] investigated the effect of the galvanic interactions on the pitting corrosion of Al-alloys. The authors used pure-Al to simulate the Al alloy matrix and two model alloys (Al–Fe and Al–Fe–Cu–Mn) to emulate the intermetallic particles. The alloys were tested in solutions of different concentrations of NaCl and NaCl + AlCl<sub>3</sub> with different pH. The Al alloys were cathodic relative to pure Al in NaCl. The effect of the surface area ratio on the galvanic current and on pitting corrosion initiation was studied. The authors concluded that the cathode area (Al alloys) determines the galvanic limiting cathodic current density and that pitting susceptibility of aluminium increases with the size of the cathode. Intergranular corrosion was also reported to occur in heat-treated Al alloys due to the simultaneous formation of precipitates in grain boundaries and of precipitates free zones (PFZ) distributed in the Al matrix. The potential difference established between the Al matrix and the precipitate rich grain boundaries or the PFZ zone was found to affect corrosion. The distribution of the precipitates at the grain boundaries as well as the composition and width of the PFZ were crucial factors affecting intergranular corrosion [8,13].

Recently, Colley et al. [14] studied the influence of Cu electrodes size on the oxygen reduction rate. These authors studied the reduction of oxygen in aqueous solutions at copper microelectrodes under mass transport conditions. The authors observed a deviation from Levich equation at high mass transport rates below a critical electrode size. This deviation was attributed to a transition from a 4 electron oxygen reduction process to a 2 electron process. These authors suggested that a similar effect may occur in Al–Cu alloys where a 2 electron process can take place on small sized

\* Corresponding author. Tel.: +351 253 510 220; fax: +351 253 516 007.  
E-mail address: [catarina.vieira@engmateriais.eng.uminho.pt](mailto:catarina.vieira@engmateriais.eng.uminho.pt) (A.C. Vieira).

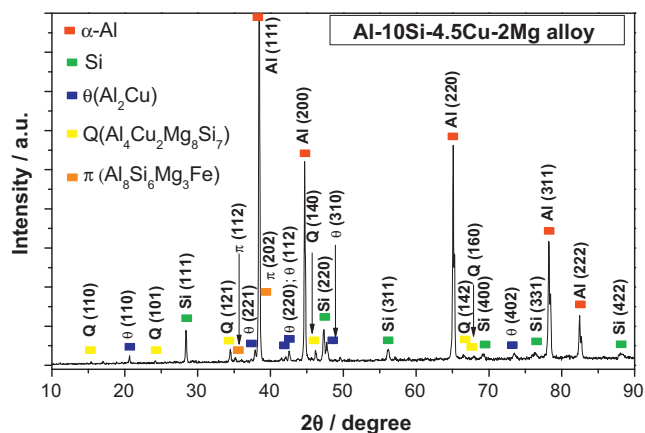


Fig. 1. XRD pattern obtained in the Al-10Si-4.5Cu-2Mg (wt.%) alloy before heat treatment. Similar XRD patterns were obtained after heat treatment.

Cu rich phases under high mass transport rates. Therefore, they anticipated an effect of Cu rich phase size distribution on oxygen reduction kinetics and thus, on corrosion of Al-Cu alloys.

The aim of this work was to gain a better insight on the role of precipitate size on the cathodic and anodic polarisation behaviour of age-hardened Al-Si-Cu-Mg alloys. Following the conclusions by Colley et al. [14], one particular goal was to evaluate to which extent the size distributions of the copper rich phases influences the oxygen reduction reaction under mass transport conditions. For that, a non-commercial Al-10Si-4.5Cu-2Mg (wt.%) alloy was cast and studied. The size of the Al<sub>2</sub>Cu phases was modified by appropriate heat-treatment. The effect of size distribution on the oxygen reduction kinetics was assessed by measuring polarisation curves in a 0.05 M NaCl solution using a rotating disk electrode.

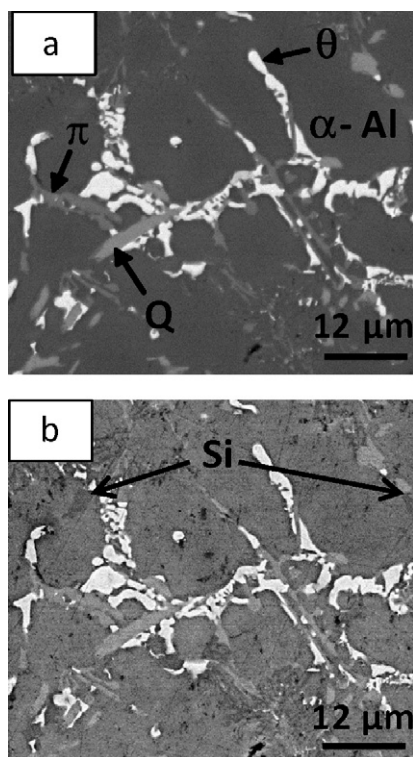


Fig. 2. SEM micrographs obtained in Al-NHT: (a) in backscattering electrons (BE) mode; (b) in secondary electrons (SE) mode. Similar phases were identified after heat treatments.

## 2. Experimental

### 2.1. Materials

A non-commercial Al-10Si-4.5Cu-2Mg (wt.%) was processed by centrifugal casting (radial geometry with 1500 rpm as centrifugal speed). The alloy was home-developed in order to present specific properties, such as good castability (by adding Si) and heat-treatment capability (by adding Cu and Mg).

Two age-hardening heat treatments were performed. In both cases, a solution heat-treatment was carried out in a tubular furnace at 500 °C followed by water quenching and artificial aging in silicone bath at 160 °C during 512 min. The solution treatment duration was either 2 h or 8 h. In this paper, the Al alloy solution treated during 2 h is identified as Al-S2h while the Al alloy solution treated during 8 h is identified as Al-S8h. To be used as reference, a non heat-treated sample was also studied and is identified as Al-NHT.

### 2.2. Structure characterization

The alloy microstructure was characterised by XRD (Cu K $\alpha$  radiation, continuous mode, scan step size of 0.02°, 2% weight detection limit, Bruker D8 Discover equipment), SEM (Nano-SEM FEI Nova 200), EDS and EDX (EDAX-Pegasus X4M). All observations and measurements were made with an acceleration voltage of 15 kV. Relative phases contents were extracted for XRD spectra (5 for each alloy) using standard software routines included in the XRD Bruker software. Prior to SEM/EDX analysis, the samples were wet-grinded up to 4000 mesh (SiC paper) and polished using 3  $\mu$ m Struers diamond spray. Phase size distribution was extracted by image analysis from SEM pictures (backscattered mode, magnification 1000, resolution 1084  $\times$  884 pixel) using Image J (Image processing and analysis in Java) software. Macro Vickers hardness measurements (30 kg, 20 s dwell time) were performed on all samples.

### 2.3. Corrosion tests

Two kinds of corrosion tests were carried out: polarisation curves of rotating disk electrodes and immersion tests. The former test gives an overview on the electrochemical kinetics as a function of the applied potential and mass transport conditions. The immersion tests were carried out in order to identify through electron microscopy corrosion patterns and related mechanisms.

The rotating disk electrodes were machined in cylindrical shape of 6 mm diameter and embedded with epoxy resin leaving exposed only one flat surface (0.283 cm<sup>2</sup>). Previous to each corrosion test, the samples were wet-polished up to 1200 mesh in SiC abrasive paper. The two types of test were carried out: immersion tests (to characterize localized corrosion mechanisms) and polarisation curves.

Immersion tests involved the immersion of the sample in the solution at open circuit potential or under anodic applied potential (-0.4 V<sub>SCE</sub>) during 30 min. Afterwards the corroded samples were analysed by SEM.

The three-electrode electrochemical cell configuration used for polarisation curves included a standard calomel reference electrode (SCE) inserted in a Luggin capillary, a Pt counter electrode and the sample connected as working electrode to the potentiostat (Autolab PGSTAT 30 under GPES software). The rotating disk electrodes were mounted with the active surface facing downwards. The Luggin capillary was placed at a distance of 6 mm below the working electrode. In this paper, all potentials are given with respect to SCE. The electrochemical solution was a 0.05 M NaCl (purity  $\geq$  99.5%, Merck) with a pH 6.2. The pH of the electrolyte was measured before and after the corrosion tests and no variation



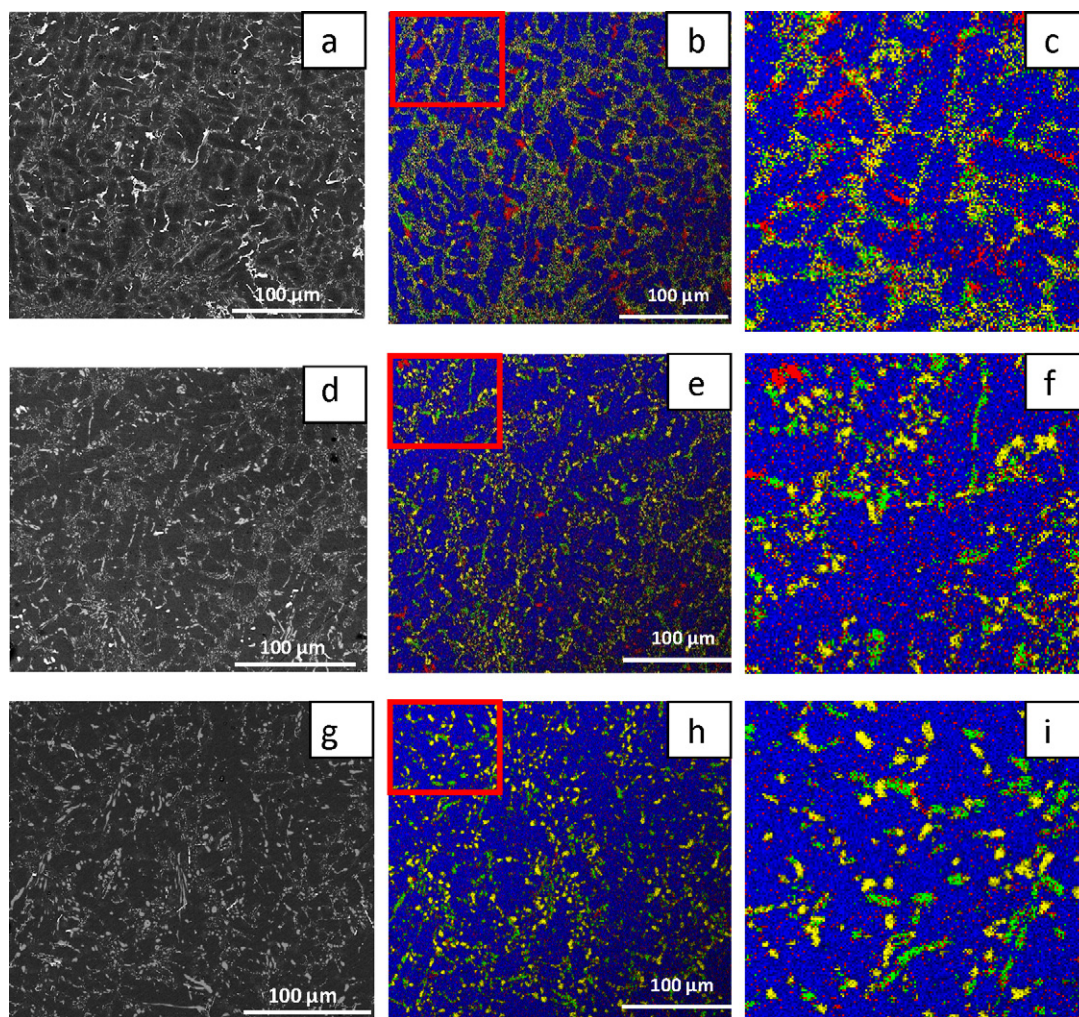


**Fig. 3.** SEM micrographs (BE mode) and EDX maps of: (a), (b) and (c) Al-NHT; (d), (e) and (f) Al-S2h; (g), (h) and (i) Al-S8h, respectively. Images (c), (f) and (i) are zoom from the marked zones. In EDX maps blue colour represents Al, red is Cu, yellow is Si and green is Mg.

was detected. The tests were carried out using a double wall cell connected to a heating bath for the purpose of keeping solution temperature constant at 25 °C. Water saturated air was continuously pumped into the solution to maintain a constant oxygen level.

Potentiodynamic polarisation measurements started from a cathodic potential of  $-0.8$  V with a potential sweep rate of 0.5 mV/s. This scan method was chosen in order to minimize surface changes possibly induced by anodic corrosion processes. The polarisation resistance was determined from polarisation curves as the slope of the linear regression of the  $E$  vs.  $j$  curves in the  $\pm 10$  mV around the corrosion potential. The samples were mounted on a Radiometer EDI101 rotating disk apparatus modified with a mercury rotating contact. Selected rotation rates were: 0 rpm, 400 rpm, 1600 rpm, 3600 rpm or 4990 rpm. For comparison, measurements were also carried out using pure Cu (Goodfellow, purity 99.99%) and pure Al (Merck, 99.99%) samples.

### 3. Results

#### 3.1. Alloys microstructure

The following constituent phases of Al-10Si-4.5Cu-2Mg (wt.%) alloy were identified in the XRD spectra (Fig. 1) before as well as after heat treatment:  $\alpha$ -Al, Si,  $\theta$ -Al<sub>2</sub>Cu, Q-Al<sub>4</sub>Cu<sub>2</sub>Mg<sub>8</sub>Si<sub>7</sub> and  $\pi$ -Al<sub>8</sub>Si<sub>6</sub>Mg<sub>3</sub>Fe.

In Al-Si-Cu-Mg alloys the precipitates can be constituted by  $\theta$ -Al<sub>2</sub>Cu, S-Al<sub>2</sub>CuMg and/or Q-Al<sub>2</sub>Cu<sub>2</sub>Mg<sub>8</sub>Si<sub>7</sub> depending on alloy composition [4–6,15]. The relative quantity of  $\theta$ -Al<sub>2</sub>Cu phase as extracted from XRD spectra of the Al-NHT samples is 5 wt%. The presence of S-Al<sub>2</sub>CuMg or  $\beta$ -Mg<sub>2</sub>Si could not be detected in the present XRD patterns. This indicates that either this phase does not form or the precipitates are of nanometric size and therefore cannot be detected by XRD.

In Fig. 2, representative SEM micrographs obtained in the Al-NHT are presented. From Fig. 2a (BSE mode), the Cu-rich phase ( $\theta$ -Al<sub>2</sub>Cu) was identified using EDS as the whitest coarse phase. The light grey phases are the intermetallic Q and  $\pi$  phases. The dark grey areas correspond to the  $\alpha$ -Al matrix. Si phase was easily identified in SE mode (Fig. 2b). The  $\theta$ -Al<sub>2</sub>Cu precipitates are the main copper containing phase, the Q phase being present only in a smaller amount.

In Fig. 3, SEM micrographs and an overlay of EDX maps obtained in the Al-NHT (Fig. 3a–c), Al-S2h (Fig. 3d–f) and Al-S8h (Fig. 3g–i) samples are presented. EDX maps and SEM micrographs were acquired in the same region. In relation to EDX maps (right columns in Fig. 3), blue colour represents Al, red is Cu, yellow is Si and green is Mg.

Both from SEM micrographs and EDX maps, Mg-containing phases (Q-Al<sub>4</sub>Cu<sub>2</sub>Mg<sub>8</sub>Si<sub>7</sub> and  $\pi$ -Al<sub>8</sub>Si<sub>6</sub>Mg<sub>3</sub>Fe) seem to have similar distribution and size in all the samples. However, the Si and the  $\theta$ -Al<sub>2</sub>Cu phases are much thinner in the heat-treated samples.

**Table 1**  
Corrosion potential values ( $E_{(j=0)}$ ) and polarisation resistance ( $R_p$ ) of Al-NHT, Al-S2h and Al-S8h measured from the polarisation curves presented in Fig. 7.

	$E_{(j=0)}$ vs SCE (V)	$R_p$ (k $\Omega$ )
Al-NHT	$-0.60 \pm 0.01$	$3.61 \pm 1.27$
Al-S2h	$-0.60 \pm 0.00$	$6.67 \pm 2.89$
Al-S8h	$-0.59 \pm 0.01$	$8.33 \pm 2.89$

The decrease in size of  $\theta$ -Al<sub>2</sub>Cu phases could be expected after age-hardening heat-treatment. Indeed, the heat treatment induces first the dissolution of the Al<sub>2</sub>Cu phase followed by its precipitation during aging in thinner entities [4,5]. Image analysis of the BE images shown in Fig. 3 reveals that 90% of the  $\theta$ -Al<sub>2</sub>Cu precipitates have size less than 2.2, 0.39 and 0.42  $\mu\text{m}^2$  for the Al-NHT, the Al-S2h and the Al-S8h, respectively. This confirms the grain refinement introduced by the heat treatment.

The formation of finer  $\theta$ -Al<sub>2</sub>Cu precipitates promotes an increase in hardness from  $\text{HV}_{30} = 109 \pm 2$  in the Al-NHT up to  $\text{HV}_{30} = 167 \pm 6$  and  $\text{HV}_{30} = 172 \pm 5$  in the Al-S2h and Al-S8h samples, respectively.

### 3.2. Immersion tests

Fig. 4 shows SEM micrographs taken on Al-S2h sample exposed for 30 min in a 0.05 M NaCl solution at open circuit potential. These micrographs are similar to what was observed in the Al-NHT and in the Al-S8h samples. The preferential dissolution in the vicinity of the  $\theta$ -Al<sub>2</sub>Cu phase grains is clearly visible (Fig. 4a). This is in agreement with the known localized corrosion mechanisms related to the galvanic coupling between the Al<sub>2</sub>Cu phase and the surrounding metal and to the pH increase due to hydroxyl ions formed during oxygen reduction [9–11]. Interestingly, the other phases (Q-Al<sub>4</sub>Cu<sub>2</sub>Mg<sub>8</sub>Si<sub>7</sub> and  $\pi$ -Al<sub>8</sub>Si<sub>6</sub>Mg<sub>3</sub>Fe) do not lead to preferential dissolution and therefore to galvanic coupling effects. Also, no effect of the Si phase can be observed (Fig. 4b). The hole observed in the micrograph presented in Fig. 4c indicates the occurrence of  $\theta$ -Al<sub>2</sub>Cu dissolution and grains pull-out due to the preferential dissolution of the surrounding matrix. The small fragments, deposited on the surface shown in Fig. 4c, were identified as  $\theta$ -Al<sub>2</sub>Cu phases by EDS. This indicates that Al<sub>2</sub>Cu fragments loosened during dissolution of the  $\theta$ -Al<sub>2</sub>Cu grains corrosion deposit on the surrounding surface. Related mechanisms were previously described [10,11,16].

The immersion test realized under an anodic applied potential ( $-0.4\text{V}$ ) was characterized by a general uniform dissolution of the surface. At microscopic level preferential matrix dissolution is observed in the vicinity of  $\theta$ -Al<sub>2</sub>Cu grains as shown in Fig. 5. No pits or any other typical appearance of pitting corrosion could be observed. No effect of heat treatment on corrosion morphology could be identified.

### 3.3. Polarisation curves at 0 rpm

In Fig. 6 four polarisation curves obtained in different tests of the Al-NHT are shown. Good reproducibility was achieved. Equivalent reproducibility was achieved with Al-S2h and Al-S8h samples. No passive plateau can be observed in the anodic domain thus, suggesting that active dissolution is the dominant corrosion mechanism.

Fig. 7 compares the polarisation behaviour of the Al-NHT, Al-S2h and Al-S8h samples. No significant differences can be detected in the cathodic domain while the anodic current between the corrosion potential and 0.3 V slightly decreases with increasing duration of the solution heat treatment.

The corrosion potential values ( $E_{(j=0)}$ ) and the polarisation resistance ( $R_p$ ) measured from the polarisation curves are presented in Table 1.  $E_{(j=0)}$  has similar values in all the samples.  $R_p$

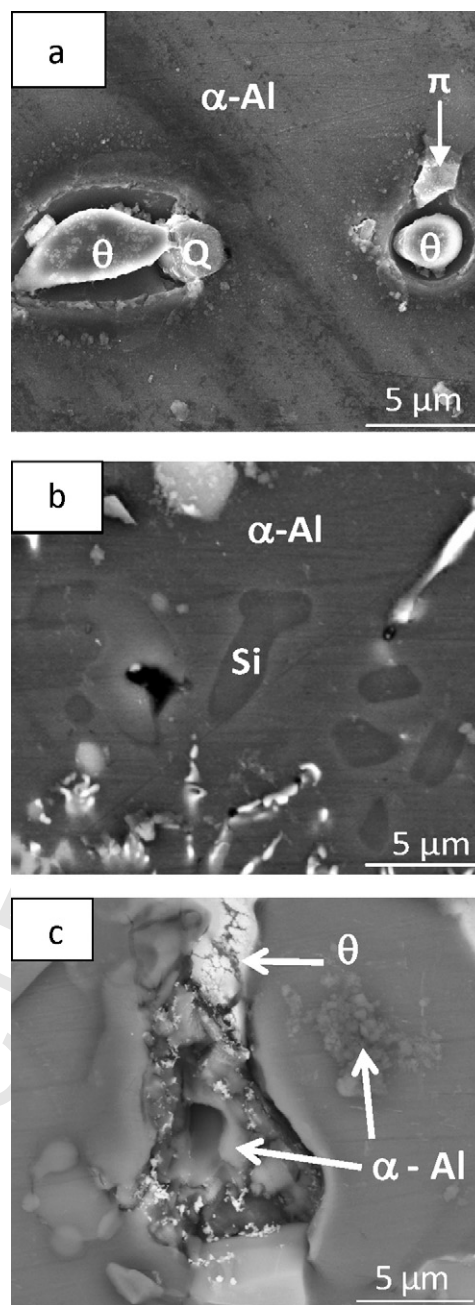


**Fig. 4.** SEM micrographs obtained after immersion tests of 30 min in 0.05 M NaCl solution: (a) in Al-S2h (BE mode); (b) in Al-S2h (SE mode); (c) in Al-NHT (BE mode). Similar micrographs were identified in Al-NHT and in Al-S8h samples.

values increase from the non heat-treated condition to the heat-treated conditions, being the highest in Al-S8h. No well defined Tafel behaviour was observed in the polarisation curves. Therefore no extrapolation of anodic or cathodic branch to the corrosion potential was performed in order to determine the corrosion current.

### 3.4. Polarisation curves of pure metals

Polarisation curves of pure Cu and pure Al in 0.05 M NaCl are presented in Fig. 8 together with the curves measured on the Al alloys. Pure Al shows the smallest cathodic current density values and the lowest corrosion potential. Its anodic behaviour is close to the one observed for the alloys. In opposition, pure Cu shows



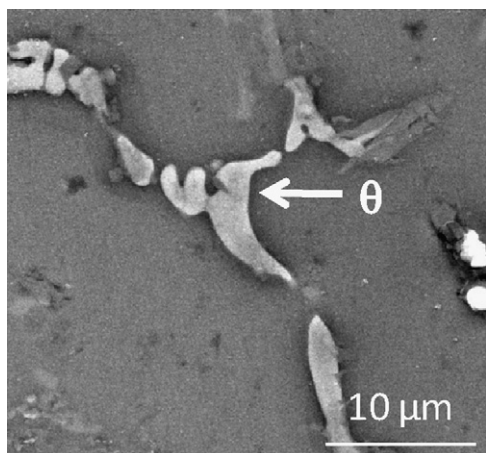


Fig. 5. SEM micrographs obtained in Al-NHT sample after anodic polarization test at  $-0.4$  V in  $0.05$  M NaCl solution during  $30$  min. Similar micrographs were identified in Al-S2h and in Al-S8h samples.

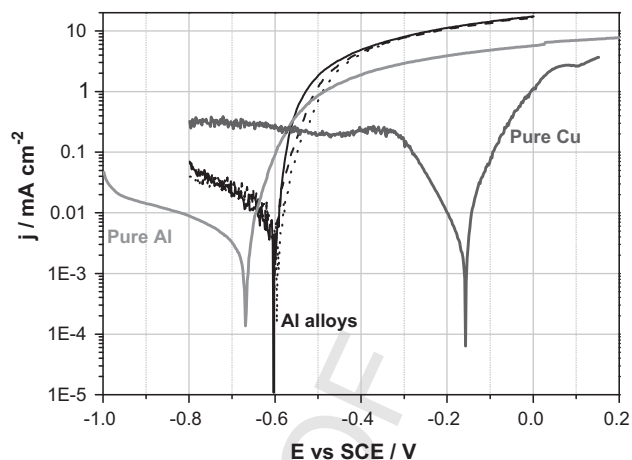


Fig. 8. Polarisation curves of pure Al, Al alloys and pure Cu in  $0.05$  M NaCl solution.

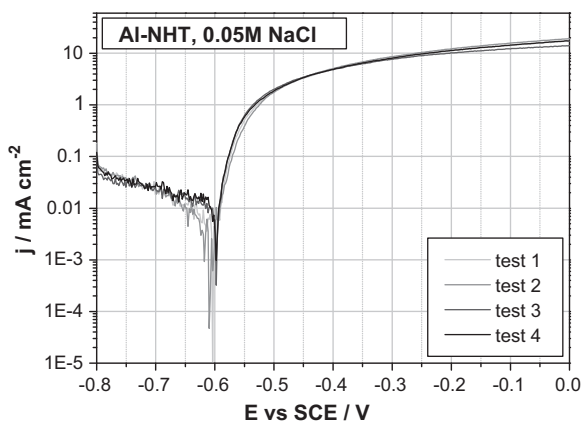
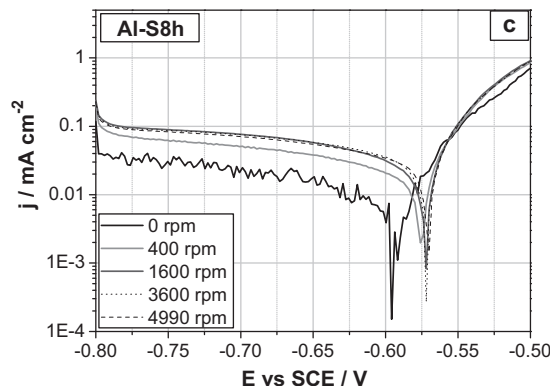
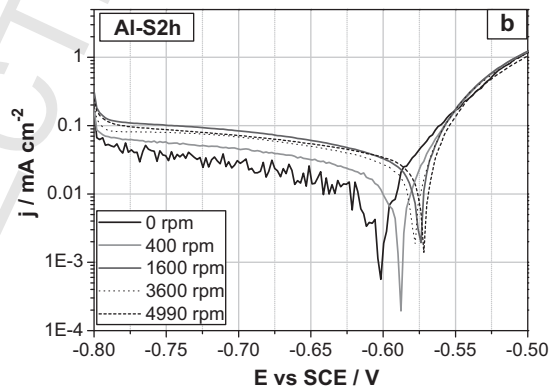
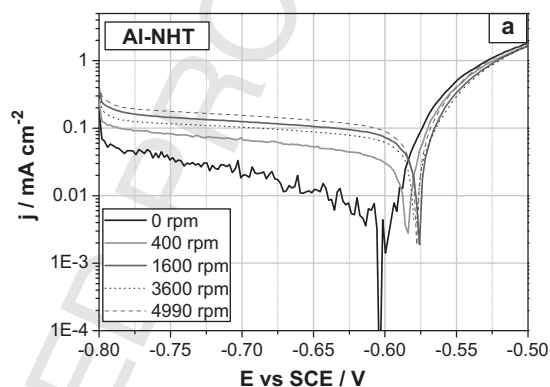


Fig. 6. Polarisation curves of the Al-NHT (without heat treatment) in  $0.05$  M NaCl. Curves obtained in 4 independent tests are shown.



the highest cathodic current densities, being its corrosion potential ( $E_{\text{corr}}$ ) value the noblest.

### 3.5. Polarisation curves under rotation

The polarisation curves obtained with  $0$ ,  $400$ ,  $1600$ ,  $3600$  and  $4990$  rpm, are presented in Fig. 9. Good reproducibility was obtained

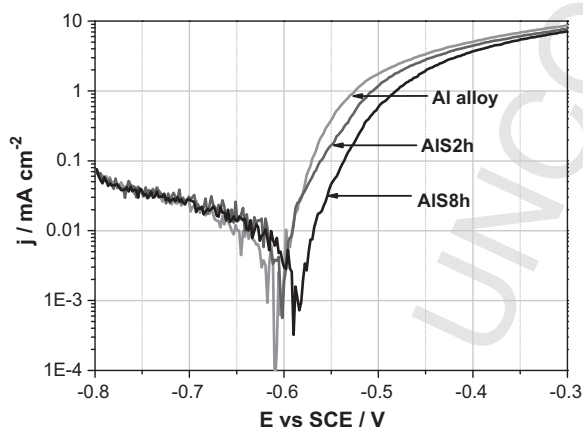


Fig. 7. Polarisation curves of Al-NHT, Al-S2h and Al-S8h samples in  $0.05$  M NaCl solution.

Fig. 9. Polarisation curves obtained with different rotating speeds in  $0.05$  M NaCl solution: (a) and (b) Al-NHT, (c) and (d) Al-S2h; (e) and (f) Al-S8h.

in all the cases. The anodic behaviour of the alloys was not affected by rotation. The cathodic current densities of the non **heat-treated** alloys (Al-NHT) increased with increasing rotation rate over all the investigated range. The **heat-treated** alloys (Al-S2h and Al-S8h) followed a similar trend up to a critical rotation rate of 1600 rpm, above which no further enhancement of the cathodic current occurred.

## 4. Discussion

### 4.1. Anodic behaviour

The anodic behaviour of the alloys is characterised, independently on alloy microstructure, by an active dissolution without any evidence of passivation or pitting (Figs. 6 and 7). Only small differences in anodic behaviour occur depending on heat treatment (Fig. 7). Ramgopal and Frankel [17] reported that the anodic current of Al-Cu alloys polarised in 0.5 M NaCl decreased with increasing concentration of copper dissolved as solid solution in the Al matrix [17]. This effect could explain the smaller current densities in the anodic domain (Fig. 7) as well as the higher polarisation resistance (Table 1) observed with the Al-S8h sample. Indeed, the solution heat treatment serves to dissolve, even only partially, the  $\theta$ -Al<sub>2</sub>Cu into the aluminium matrix. The longer solution heat treatment used for Al-S8h samples lead to more copper being dissolved in solid solution [6,18,19]. The age hardening treatment serves to precipitate the  $\theta$ -Al<sub>2</sub>Cu phase out of the solid solution. Since, age hardening is identical for the Al-S2h and Al-S8h samples, one would expect higher residual copper contents and thus lower anodic currents in the matrix of the Al-S8h sample. According to this mechanism one would conclude that the Al-NHT contains less copper in solid solution than the **heat-treated** samples. Although reports from the literature lend support to this hypothesis [6,18], only chemical analysis of the matrix would provide confirmation. However, the determination of the copper concentration in the matrix is complex and requires the use of sensitive, high lateral resolution techniques. This goes beyond the scope of the present article.

### 4.2. Cathodic behaviour

The present results confirm that  $\theta$ -Al<sub>2</sub>Cu phases act as preferential cathodes causing galvanic coupling and preferential dissolution of the Al matrix surrounding them (Figs. 4 and 5). The cathodic current densities measured on pure Al are one order of magnitude lower than the corresponding values found for the Al alloys (Fig. 8). This is indicative of a poor catalytic effect of aluminium on the oxygen reduction reaction. Copper apparently act as catalyser for the cathodic reaction. Interestingly the cathodic current on pure copper is, depending on potential, one to two orders of magnitude larger than in the alloys. This lends support to the conclusion that the copper  $\theta$ -Al<sub>2</sub>Cu phase constitutes the main site of cathodic reduction. Indeed the other phases (including the copper bearing Q-Al<sub>4</sub>Cu<sub>2</sub>Mg<sub>8</sub>Si<sub>7</sub> phase) do not induce preferential dissolution of the aluminium matrix (Fig. 4) and **thus, apparently** do not act as cathodes.

Mass transport conditions largely affect the cathodic kinetics. At low rotation rates (below 1600 rpm) no differences can be observed between the different samples while at higher rates the behaviour of the Al-S2h and Al-S8h diverges from the non treated alloy.

To best illustrate this phenomenon, the cathodic current density at  $-0.7$  V was plotted as a function of the square root of the rotation rate (angular velocity) of the disk electrode in a Levich plot (Fig. 10). In accordance to literature [20,21] the reaction kinetics is mass transport controlled when the limiting current density varies linearly with the rotating rate square. Such linearity is indeed

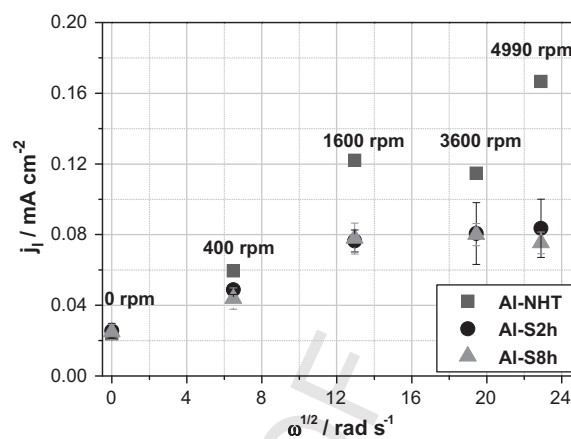


Fig. 10. Variation of the cathodic limiting current with rotation rate square in 0.05 M NaCl solution, for Al-NHT, Al-S2h and Al-S8h samples ( $j_l$  values were obtained for  $E = -0.7$  V).

generally observed in the Levich plot of the non heat-treated alloy (Al-NHT) on the whole rotation rate range. The **heat-treated** alloys (Al-S2h and Al-S8h) exhibit a linear variation up to a critical rotation rate of 1600 rpm above which a plateau is observed.

Fig. 10 shows that the non **heat-treated** alloy follows quite well the linear behaviour predicted by the Levich equation. However, the intercept with the current axis in Fig. 10 is not zero indicating a mixed control of the cathodic reaction. Usually two reactions ((1) and (2)) contribute to the cathodic current:



The former reaction (1) is usually mass transport controlled due to the low solubility of oxygen in water except in presence of strong inhibiting surface such as passive electrodes where the kinetics can be limited by charge transfer. Thus, in the present situation reaction (1) can be under mixed control. The water reduction reaction (2) is usually under charge transfer control. However, no reliable kinetics data are available to assess the relative contribution of reactions ((1) and (2)) to the charge transfer controlled reduction on these aluminium alloys.

The theoretical limiting current density for oxygen reduction can be calculated using the Levich Eq. (3):

$$j_l = 0.62nF C_B D_B^{2/3} \nu^{-1/6} \omega^{0.5} \quad (3)$$

where  $j_l$  is the limiting current density in A/cm<sup>2</sup>,  $F$  is the Faraday constant in C/eq,  $C_{B,b}$  is the concentration of B in the bulk in mole/cm<sup>3</sup> (B is the minor specie involved in the reaction),  $D_B$  is the diffusion coefficient in cm<sup>2</sup>/s,  $\nu$  is the kinematics viscosity in cm<sup>2</sup>/s,  $\omega$  represents the angular velocity in rad/s and  $n$  is the apparent number of electrons (eq/mol). From standard literature [20], following typical values can be assumed:  $n = 4$  eq/mol,  $F = 96485$  C/eq,  $\text{CO}_2 = 2.52 \times 10^{-7}$  mol/cm<sup>3</sup>,  $\text{DO}_2 = 2.51 \times 10^{-5}$  cm<sup>2</sup>/s (for oxygen in water),  $\nu = 0.01$  cm<sup>2</sup>/s. One can thus calculate the limiting current as a function of rotation rate  $\omega$ . Table 2 presents the calculated theoretical values together with the experimental currents measured at  $-0.7$  V. The theoretical data largely exceeds the observed values that constitutes in average only 3–8% of the expected current. This fraction corresponds well with the  $\theta$ -Al<sub>2</sub>Cu phase relative quantity of 5% determined by XRD. Thus, one can conclude that oxygen reduction occurs essentially on this copper rich phase.

The cathodic polarisation behaviour of the pure element lends support to this hypothesis. Indeed, the reduction reaction on pure aluminium is very low compared to the alloy. The slope of the curve indicates that the reaction is under charge transfer control.



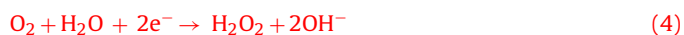
**Table 2**

Theoretical limiting current values considering a 4 electron oxygen reduction reaction and experimental limiting current values for Al-NHT, Al-S2h and Al-S8h samples. Data in parentheses indicate the ratio (%) between experimental and the theoretical values.

Rotation rate (rpm)	Theoretical $j_L$ (mAcm <sup>-2</sup> )	Al-NHT	Al-S2h	Al-S8h
0	0	0.024	0.026	0.025
400	0.72	0.060 (8.3)	0.049 (6.8)	0.044 (6.1)
1600	1.44	0.122 (8.5)	0.076 (5.3)	0.078 (5.4)
3600	2.16	0.115 (5.3)	0.081 (3.7)	0.080 (3.7)
4990	2.55	0.167 (6.5)	0.084 (3.3)	0.075 (3.0)

In pure Cu the current exhibits a plateau at relatively high value of 0.2 mA cm<sup>-2</sup> well corresponding to the limiting current for oxygen reduction at low rotation rates. Indeed, in chlorides systems the oxygen reduction is known to dominate the cathodic reaction on copper electrodes while the contribution of cathodic hydrogen evolution appears at potentials more negative than -1.0 V vs. SCE [22]. Possibly, oxygen reduction on pure aluminium, and thus on the alloy matrix, is inhibited by passivating surface films [20] or other corrosion products [23,24].

The mass transport behaviour of the aged alloys (Al-S2h and Al-S8h) differs from the non heat-treated alloy (Al-NHT). First, a plateau appears above 1600 rpm in Fig. 10. This indicates that the mass transport rate on Al-S2h and Al-S8h samples is high enough for the charge transfer becoming the limiting factor. Secondly, the oxygen reduction reaction on age-hardened alloys is less efficient even below 1600 rpm where kinetics is mass transport controlled. In fact the ratio between experimental and theoretical current (Table 2) for the Al-NHT samples is approximately twice the ratio found on the other samples. These differences in behaviour should be related to the different microstructures obtained through the heat treatments, in particular the size distribution of the  $\theta$ -Al<sub>2</sub>Cu phase. Colley et al. [14] found a decreasing oxygen reduction kinetics under high mass transport rates with decreasing cathode size due to a transition from a 4 (reaction (1)) to a 2 electron process (reaction (4) followed by reaction (5)).



Under high mass transport rates the H<sub>2</sub>O<sub>2</sub> molecules as intermediate compounds are removed from the electrode before they can reduce. Hydrogen peroxide decomposes according to reaction (5) afterwards in the bulk solution without contributing to the electrode process. Thus, a ratio of 2 between the 4 electron process current (Al-NHT) and 2 electron process current (Al-S2h and Al-S8h) is anticipated and supported by the current ratios listed in Table 2. In absence of rotation a 4 electron mechanisms should take place independently on microstructure. This is indeed observed in the present experiments (Fig. 7).

The hypothesis of Colley et al. [14] gives a reasonable explanation to the present results. However, other phenomena may be influenced by mass transport. The redistribution of copper as observed in Fig. 5 implies a mass transfer that is possibly affected by electrode rotation. Under rotation, dissolved copper may be transported away from the electrode before it can re-deposit. This may reduce the amount of copper at the surface and thus the oxygen current. The size distribution of the Al<sub>2</sub>Cu particles may affect the local copper concentration gradient and thus, the transport phenomena and eventually re-deposition. However, the redistribution mechanisms are not sufficiently known to reasonably predict the effect of rotation. Nevertheless the present results are quite accurately described by the oxygen reaction kinetics so that the possible influence of re-deposition seems to be of secondary relevance.

### 4.3. Effect of heat treatment on corrosion

The present results clearly show that both the cathodic and anodic kinetics of the Al-10Si-4.5Cu-2Mg alloy are affected by the heat treatments and by the mass transport conditions. As a consequence the heat treatment is expected to influence the corrosion behavior depending on the flow conditions established in the electrolyte.

In absence of significant mass transport, the kinetics of the oxygen reduction is not significantly affected by the heat treatment (Fig. 10) and thus, by the alloy microstructure. On the other hand anodic current of the heat-treated alloys is slightly smaller compared to the untreated alloy (Fig. 7). As a consequence the corrosion rate i.e. the anodic current at the corrosion potential (where the cathodic and anodic kinetics are at equilibrium), is expected to be larger in absence of heat treatment. This is indeed confirmed by the higher polarization resistances (Table 1) measured after heat treatment.

For all alloys, increasing mass transport results in an acceleration of the oxygen reduction kinetic (Fig. 10), leading to more anodic corrosion potentials and larger corrosion rates. Note that the mass transport has little effect on the anodic oxidation of the alloys (Fig. 9). The heat treatment has a major effect on the evolution with mass transport of the kinetics of the oxygen reduction kinetics. The smaller Al<sub>2</sub>Cu preferential cathodes formed in the heat-treated alloys promote a transition from a 4 electron to a 2 electron process at high mass transport rates [14]. Further the limiting current levels off at higher rotation rates in the case of the heat-treated alloys only (Fig. 10). For both reasons, the cathodic reaction and thus, the corrosion rate are expected to be significantly higher in the non heat-treated alloy compared to the alloys after solution treatment and artificial aging. This effect manifest however itself only at high mass transport rates while in static solutions the effect of heat treatment on corrosion is the smallest.

## 5. Conclusions

The polarisation behaviour of a cast Al-10Si-4.5Cu-2Mg alloy was investigated in NaCl 0.05 M using a rotating disk electrode with the aim to identify the role of  $\theta$ -Al<sub>2</sub>Cu phase size distribution on the corrosion behaviour. Three different  $\theta$ -Al<sub>2</sub>Cu phase size distributions were achieved by appropriate age hardening heat treatments. From this study, the following conclusions can be drawn:

- The heat treatment only slightly affected the anodic behaviour of the alloy that is characterised by an active like dissolution mechanisms independent of mass transport conditions. The slight reduction in anodic current observed after heat treatments was attributed to the differences in the amount of residual copper dissolved in the Al matrix.
- The cathodic reactions were identified as kinetically limited water reduction as well a mass transport controlled oxygen reduction. The  $\theta$ -Al<sub>2</sub>Cu phase acts as preferential cathode essentially because the oxygen reduction takes place there.
- The Al<sub>2</sub>Cu phase size distribution affected the mass transport dependent kinetics of oxygen reduction. The coarse structure exhibited the mass transport dependence predicted by the Levich equation for a 4 electron oxygen reduction process taking place on the  $\theta$ -Al<sub>2</sub>Cu phases. The fine size distribution achieved by the age hardening treatment seems to promote a 2 electron process that follows Levich equation up to a rotation rate of 1600 rpm. Above this value, the oxygen reduction rate is kinetically limited.

478 **Acknowledgments**

479 The research team was financially supported by the Portuguese  
480 Foundation for Science and Technology (FCT–Portugal), under a  
481 PhD scholarship (SFRH/BD/27911/2006). The authors thank also to  
482 Drs. Edith Ariza (University of Minho) and Pierre Mettraux (EPFL)  
483 for SEM analysis.

484 **References**

- 485 [1] F. Grosselle, G. Timelli, F. Bonollo, *Materials Science and Engineering A* 527  
486 (2010) 3536.
- 487 [2] W.S. Miller, L. Zhuang, J. Bottema, A.J. Wittebrood, P. De Smet, A. Haszler, A.  
488 Vieregge, *Materials Science and Engineering A* A280 (2000) 37.
- 489 [3] E. Schubert, M. Klassen, I. Zerner, C. Walz, G. Sepold, *Journal of Materials Tech-*  
490 *nology* 115 (2001) 2.
- 491 [4] R.X. Li, R.D. Li, Y.H. Zhao, L.Z. He, C.X. Li, H.R. Guan, Z.Q. Hu, *Materials Letters* 58  
492 (2004) 2096.
- 493 [5] G. Wang, Q. Sun, L. Feng, L. Hui, Cainian Jing, *Materials and Design* 28 (2007)  
494 1001.
- 495 [6] L. Lasa, J.M. Rodriguez-Ibabe, *Materials Characterization* 48 (2002) 371.
- 496 [7] A. Gaber, M.A. Gaffar, M.S. Mostafa, E.F. Abo Zeid, *Journal of alloys and com-*  
pounds 429 (2007) 167.
- [8] M. Kappes, L. Kovarik, M.J. Mills, G.S. Frankel, M.K. Miller, *Journal of The Elec-*  
trochemical Society 155 (2008) C437.
- [9] Z. Szklarska-Smialowska, *Corrosion Science* 41 (1999) 1743.
- [10] N. Birbilis, R.G. Buchheit, *Journal of The Electrochemical Society* 152 (2005)  
B140.
- [11] K.S. Rao, K.P.D. Rao, *Transactions of the Indian Institute of Metals* 57 (2004)  
593.
- [12] C. Liao, R.P. Wei, *Electrochimica Acta* 45 (1999) 881.
- [13] V. Guillaumin, G. Mankowski, *Corrosion Science* 42 (2000) 105.
- [14] A.L. Colley, J.V. Macpherson, P.R. Unwin, *Electrochemistry Communications* 10  
(2008) 1334.
- [15] D.J. Chakrabarti, D.E. Laughlin, *Progress in Materials Science* 49 (2004) 389.
- [16] Q. Meng, G.S. Frankel, *Journal of the Electrochemical Society* 151 (2004) B271.
- [17] T. Ramgopal, G.S. Frankel, *Corrosion* 57 (2001) 702.
- [18] E. Sjolander, S. Seifeddine, *Journal of Materials Processing Technology* 210  
(2010) 1249.
- [19] F.J. Tavitias-Medrano, A.M.A. Mohamed, J.E. Gruzleski, F.H. Samuel, H.W. Doty,  
*Journal of Material Science* 45 (2010) 641.
- [20] D. Landolt, *Corrosion and Surfaces Chemistry of Metals*, 1st ed., EPFL Press,  
2007.
- [21] S. Han, J. Zhai, L. Shi, X. Liu, W. Niu, H. Li, G. Xu, *Electrochemistry Communica-*  
tions 9 (2007) 1434.
- [22] G. Kear, B.D. Barker, F.C. Walsh, *Corrosion Science* 46 (2004) 109.
- [23] B. Zaid, D. Saidi, A. Benzaid, S. Hadji, *Corrosion Science* 50 (2008) 1841.
- [24] S.M. Moon, S.I. Pyun, *Corrosion Science* 39 (1997) 399.

497  
498  
499  
500  
501  
502  
503  
504  
505  
506  
507  
508  
509  
510  
511  
512  
513  
514  
515  
516  
517  
518  
519  
520  
521